JOURNAL OF GEOPHYSICAL RESEARCH, VOL. 106, NO. B10, PAGES 21,785–21,798, OCTOBER 10, 2001

Marginal stability of atmospheric eruption columns and pyroclastic flow generation

Édouard Kaminski and Claude Jaupart

Institut de Physique du Globe de Paris, Paris, France

Abstract. Explosive volcanic eruptions frequently generate fall and flow deposits simultaneously, which can be attributed to a marginally stable atmospheric column in transitional conditions between the buoyant and collapse regimes. This behavior is reproduced by laboratory experiments and numerical simulations. Ten well-documented eruptions are used to test theoretical models of explosive eruptions. Three types of deposits, fall, flow, and composite deposits made of intercalated flow and fall units, are observed in these eruptions. Estimates of mass discharge rate and initial volatile concentration in the magma are available for each eruptive phase. Using the simple assumptions that (1) the mass fraction of gas in the mixture is equal to the initial volatile content of magma and (2) jet expansion outside the vent is unconstrained by crater dimensions, theoretical predictions are not consistent with the data. Agreement between data and theory may be achieved by appealing to imperfect degassing of pyroclasts, which lowers the gas content of the erupted mixture. The effective amount of continuous gas phase carrying pyroclasts in suspension depends on the size distribution of pyroclasts. In coarse pyroclast populations a large amount of magmatic gas remains trapped in bubbles within the pyroclasts and is not involved in the bulk volcanic flow. A new regime diagram based on estimates of the effective gas content in the erupted mixture allows good agreement with the observations. For given mass flux and initial dissolved volatile content, changes of the size distribution of pyroclasts may have a strong effect on atmospheric column behavior.

1. Introduction

Explosive eruptions discharge huge amounts of pyroclasts carried by turbulent gas jets and generate tephra deposits. Two end-member types of deposits have been associated with different regimes for the atmospheric eruption column. Fall deposits cover large areas and are generated by the settling of pyroclasts from an umbrella cloud fed by a high-altitude eruption column. Flow deposits are usually confined to valleys and record complex depositional processes. Some flows are due to the explosion of silicic lava domes and others are due to avalanches of pyroclasts issued from eruption columns, but we shall only deal with the latter kind here. According to theory, pyroclastic flow generation is due to the collapse of an eruption column which exhausts its upward momentum [*Sparks and Wilson*, 1976]. Field observations show more complexity. Pyroclastic deposits are often made of intercalated flow and fall units, e.g., Novarupta 1912 [*Hildreth*, 1987], Mount St. Helens 1980 [*Criswell*, 1987], Taupo 1.8 ka B.P. [*Wilson and Walker*, 1985], and Bishop Tuff 0.76 Ma [*Wilson and Hildreth*, 1997]. Laboratory and numerical experiments demonstrate that such characteristics can be generated by unstable Plinian columns in transitional conditions between the buoyant and collapse regimes [*Carey et al.*, 1988; *Valentine and Wohletz*, 1989; *Woods and Caulfield*, 1992; *Neri and Dobran*, 1994; *Ernst et al.*, 1996].

For the purpose of comparing model predictions and observations it is useful to define three different regimes for an atmospheric column. In the "buoyant" regime the eruption column rises to large heights above the vent, with only a few weak and dilute currents cascading from its edges. The end result is a widespread fall deposit with volumetrically insignificant flow components. When eruption conditions are close to those of column collapse, a buoyant column still extends to high altitudes, but it is unstable and generates powerful dense currents. In this "transitional" regime fall and flow deposits are produced simultaneously. Finally, the "collapse" regime is such that the column does not rise to large heights and does not feed an umbrella cloud but forms a collapsing fountain feeding pyroclastic flows. The end result is a "pure" flow deposit without intercalated fall units.

Paper number 2001JB000215
0148-0227/01/2001JB000215$09.00.

Theoretical models provide a quantitative link between field data and eruption characteristics. The eruption regime may be defined by the values of three variables at the base of the atmospheric column: the mass fraction of gas, the mean vertical velocity, and the column radius [*Wilson et al.*, 1980; *Woods*, 1995]. For an ancient eruption one may determine the values of only two variables, the mass discharge rate, which is determined from the characteristics of the pyroclastic deposit, and the total volatile content of magma, which may be obtained from phase equilibria and melt inclusion studies. In the influential study of *Wilson et al.* [1980], models of conduit flow were used to determine relationships between eruption velocity and gas content. One piece of information is lacking, the relationship between gas content at the vent and the total volatile concentration in the magma. The simplest procedure is to equate the two, i.e., to assume that all the volatiles exolve and collect into the gas phase. This framework has been applied to the eruptions of Vesuvius, Mount St. Helens, and Bishop Tuff [*Carey and Sigurdsson*, 1987; *Carey et al.*, 1990; *Gardner et al.*, 1991]. Model calculations predict that the atmospheric columns were well into the buoyant regime and fail to account for the production of pyroclastic flows, contrary to field observations. This suggests that the theoretical models are flawed or that the input parameters were not estimated correctly.

In this paper, we review the basic elements of the theory and assess uncertainties in the quantitative predictions. We review data and observations on 10 well-documented eruptions and compare them to theoretical predictions. Most fluid dynamical models have been aimed at predicting flow conditions for given gas contents. Here we stress that one also needs to evaluate properly the relationship between the effective gas content of the erupting mixture and the total volatile content of the initial magma. We show that errors on the gas content may be more critical than errors on the fluid dynamical models. We propose a new regime diagram which accounts for the observations.

2. Ten Well-Studied Eruptions

We review a number of eruptions for which field observations are sufficient for a reconstruction of the eruptive history and reliable estimates of mass flux and for which the volatile concentration of the initial magma is known. These eruptions were chosen to encompass a large range of mass discharge rate and volatile content. All the available data are summarized in Table 1.

2.1. The 1980 Mount St. Helens

Detailed observations have been made for the Mount St. Helens eruption sequence on May 18, 1980 [e.g., *Carey et al.*, 1990]. Mount St. Helens started with two pure buoyant phases (B1-B2 units) with an increasing mass discharge rate and then produced strong pyroclastic flows from a relatively high column (B3 unit) before returning to a pure buoyant phase (B4 unit). This sequence has been established after careful comparisons between direct observations of the eruption, atmospheric radar data, and studies of the pyroclastic deposits. Especially noteworthy is the decrease of column height (as determined from the radar data) which occurs as the eruption starts producing pyroclastic flows. At that point in time, the eruption went close to collapse conditions and is best described as making an incursion into the transitional regime. Mass discharge rate estimates for the buoyant phases were consistent with column heights detected by radar [*Carey et al.*, 1990]. The careful reconstruction of the eruption sequence and detailed volumetric studies of the pyroclastic deposit allow an estimate of the average mass discharge rate in the transitional phase [*Carey et al.*, 1990]. The initial magma had 4.6 wt % water and 40% phenocrysts [*Rutherford et al.*, 1985], and the deposits contain $\approx$ 10% lithics [*Carey and Sigurdsson*, 1982].

2.2. Vesuvius 79 AD

Vesuvius followed an evolution similar to that of Mount St. Helens, starting with a buoyant column producing several fall layers (levels 0.25W, 0.5W, 0.75W and 1W of the white fall sequence) and evolving toward more unstable conditions with the generation of surges when magma composition changed (levels W/G-S1, S1-S2, S2-S3, S3-S4 of the gray fall sequence) [*Carey and Sigurdsson*, 1987]. These later phases were characterized by the largest mass discharge rates and are best described as transitional. The volatile contents of successive phases were estimated for the changing proportions of "white" and "gray" magmas [*Sigurdsson et al.*, 1990]. The gray magma contained 18% phenocrysts and 4.7 wt % water, while the white magma contained 27% phenocrysts and 3.5 wt % water. There were $\approx$10% lithics in the flow [*Sigurdsson et al.*, 1985].

2.3. The 1912 Novarupta-Katmai

The Novarupta-Katmai eruption produced numerous intercalated fall and flow deposits. During the first episode (episode I, layers A and B of *Fierstein and Hildreth* [1992]), the eruption evolved from a dominantly buoyant regime with small pyroclastic flows (layer A in the deposit) to an unstable phase with numerous ash flows (layer B). At the same time, the magma composition was changing, from water-rich rhyolite to a mixture of rhyolite and less evolved magmas with smaller volatile contents [*Westrich et al.*, 1991]. Thus, in this case, the change of eruption regime coincided with a change of volatile content. There was no sustained pure pyroclastic flow phase, except perhaps at the very end of episode I, when a small andesite-rich ash flow unit was deposited. The intercalation of fall and flow units [*Fierstein and Hildreth*, 1992] indicates an unstable column and suggests a transitional regime. Episode I ended by the collapse of the summit caldera, which was recorded

Table 1. Eruption Conditions[a]

Eruption (Deposit)	M, kg s^{-1}	n_o, wt %	α_c, %	x_o, wt %	x_f, wt %	Rg
Mount St. Helens 1980 (B1)	6.3×10^6 (1)	4.6 (2)	50 (2,3)	2.3	1.5	B
Mount St. Helens 1980 (B2)	1.3×10^7 (1)	4.6 (2)	50 (2,3)	2.3	1.5	B
Mount St. Helens 1980 (B3)	4.4×10^7 (1)	4.6 (2)	50 (2,3)	2.3	1.5	T
Mount St. Helens 1980 (B4)	1.6×10^7 (1)	4.6 (2)	50 (2,3)	2.3	1.5	B
Vesuvius 79 (0.25W)	6.1×10^6 (4)	4.7 (5)	28 (5,6)	3.4	2.2	B
Vesuvius 79 (0.5W)	9.2×10^6 (4)	4.6 (5)	29 (5,6)	3.3	2.1	B
Vesuvius 79 (0.75W)	1.7×10^7 (4)	4.5 (5)	29 (5,6)	3.2	2.1	B
Vesuvius 79 (1W)	7.1×10^7 (4)	4.0 (5)	32 (5,6)	2.7	1.7	B
Vesuvius 79 (W/G-S1)	1.5×10^8 (4)	3.5 (5)	37 (5,6)	2.2	1.3	T
Vesuvius 79 (S1-S2)	4.7×10^7 (4)	3.5 (5)	37 (5,6)	2.2	1.3	T
Vesuvius 79 (S2-S3)	10^8 (4)	3.7 (5)	36 (5,6)	2.4	1.5	T
Vesuvius 79 (S3-S4)	9.4×10^6 (4)	3.6 (5)	36 (5,6)	2.3	1.4	T
Katmai-Novarupta (A)	10^8 (7)	4.0 (9)	8 (7,9)	3.7	2.3	T
Katmai-Novarupta (B)	4.2×10^8 (8)	3.0 (9)	12 (7,9)	2.6	1.6	T
Katmai-Novarupta (CD)	2×10^8 (7)	2.6 (9)	32 (7,9)	1.8	1.0	T
Katmai-Novarupta (FG)	4×10^7 (7)	2.6 (9)	42 (7,9)	1.5	0.8	T
Taupo (Y2)	1.8×10^8 (10)	4.3 (11)	20 (11,12)	3.4	2.2	B
Taupo (Y5-6)	1.1×10^9 (10)	4.3 (11)	20 (11,12)	3.4	2.2	T
Taupo (Y7)	7.7×10^9 (10)	4.3 (11)	20 (11,12)	3.4	2.2	C
Nevado del Ruiz	5×10^7 (10)	3.0 (13)	60 (13,14)	1.2	0.7	T
Tambora (F2)	1.1×10^8 (15)	2.3 (15)	23 (15)	1.8	1.0	B
Tambora (F4)	2.8×10^8 (15)	2.6 (15)	23 (15)	2.0	1.1	B
Tambora (F5-S1)	5×10^8 (15)	1.4 (15)	23 (15)	1.1	0.5	C
Minoan (Phase 1)	2.5×10^8 (16)	6.0 (16)	25 (17,18)	4.5	3.1	B
Fogo A	10^8 (10)	2.9 (19)	19 (19,20)	2.3	1.4	T
El Chichon (A)	8×10^7 (10)	6.0 (21)	45 (22)	3.3	2.3	B
El Chichon (B)	1.5×10^8 (10)	6.0 (21)	45 (22)	3.3	2.3	T
El Chichon (C)	8.5×10^7 (10)	6.0 (21)	45 (22)	3.3	2.3	T
Bishop Tuff (F1)	2×10^7 (23)	5.7 (24)	15 (25)	4.8	3.3	B
Bishop Tuff (F2)	1.2×10^8 (23)	5.7 (24)	15 (25)	4.8	3.3	T
Bishop Tuff (F3)	1.2×10^8 (23)	5.7 (24)	15 (25)	4.8	3.3	T
Bishop Tuff (F4)	1.2×10^8 (23)	5.7 (24)	15 (25)	4.8	3.3	T
Bishop Tuff (F5)	2×10^8 (23)	5.7 (24)	15 (25)	4.8	3.3	T
Bishop Tuff (F6)	2×10^8 (23)	5.7 (24)	15 (25)	4.8	3.3	T
Bishop Tuff (F7)	8×10^8 (23)	5.7 (24)	15 (25)	4.8	3.3	T
Bishop Tuff (F8)	2×10^8 (23)	5.7 (24)	15 (25)	4.8	3.3	T
Bishop Tuff (F9)	2×10^8 (23)	4.1 (24)	15 (25)	3.5	2.2	T

[a] M is the mass discharge rate (peak value for eruptions in the transitional or buoyant regime and average value for eruptions in the collapse regime), n_o is the total volatile content of the melt, α_c is the percentage of crystals in the melt plus lithics in the flow, x_o is the mass fraction of gas in the mixture (liquid+phenocrysts+lithics+gas) for complete degassing, x_f is the mass fraction of exsolved gas in the mixture at fragmentation for a threshold vesicularity of 70%, Rg is the column regime: B, buoyant; T, transitional; and C, collapse. Numbers in parentheses are the references: 1, *Carey et al.* [1990]; 2, *Rutherford et al.* [1985]; 3, *Carey and Sigurdsson* [1982]; 4, *Carey and Sigurdsson* [1987]; 5, *Sigurdsson et al.* [1990]; 6, *Sigurdsson et al.* [1985]; 7, *Fierstein and Hildreth* [1992]; 8, *Hildreth* [1991]; 9, *Westrich et al.* [1991]; 10, *Carey and Sigurdsson* [1989]; 11, *Dunbar et al.* [1989]; 12, *Wilson and Walker* [1985]; 13, *Melson et al.* [1990]; 14, *Naranjo et al.* [1986]; 15, *Sigurdsson and Carey* [1989]; 16, *Sparks and Wilson* [1989]; 16, *Cottrell et al.* [1999]; 17, *Druitt et al.* [1989]; 18, *Pyle* [1989]; 19, *Gardner et al.* [1996]; 20, *Walker and Croasdale* [1970]; 21, *Luhr* [1990]; 22, *Sigurdsson et al.* [1987]; 23, this study; 24, *Wallace et al.* [1999]; 25, *Gardner et al.* [1991].

by seismometers. Using the available time constraints, *Hildreth* [1991] has estimated a mass eruption rate of 4.2×10^8 kg s^{-1} for the emplacement of phase B ignimbrite. Later phases (episode II, layers C and D, and episode III, layers F and G) probably also belong to the transitional domain because there were several ash flows while a fall deposit was accumulating [*Fierstein and Hildreth*, 1992]. The last major phases (layers F and G) involved mostly dacitic magma with smaller water contents and smaller discharge rates than the first major phase. The volatile contents of successive phases can be estimated for the changing proportions of andesitic, dacitic, and rhyolitic magmas, containing 1.2 wt %, 2.5 wt %, and 4 wt % water, respectively [*Westrich*

et al., 1991]. Layers A, B, C-D, and F-G contain 3%, 10%, 30%, and 40% phenocrysts, respectively, and 5% lithics [*Fierstein and Hildreth*, 1992].

2.4. Taupo

The Taupo eruption led to a complex deposit, labeled Y by *Wilson* [1993]. Its first major phase (Hatepe Y2) generated a uniform, nongraded and well-sorted fall deposit, which must therefore be attributed to a buoyant column. The eruption then went through a complex succession of phreatomagmatic phases. During the deposition of units Y5 and Y6 it returned to dry conditions with no external water involved. At that stage the eruption was probably in a transitional regime because ignimbrite layers are intercalated with fall units, indicating that many pyroclastic flows were perturbing the accumulation of the fall deposit. The eruption eventually switched to a major pyroclastic flow phase which led to the deposition of the large Taupo Ignimbrite (unit Y7). This phase was therefore in the collapse domain. There was no detectable change of magma volatile content as the eruption regime was changing [*Dunbar et al.*, 1989]. The mass discharge rates for the two main phases have been estimated using various techniques. *Carey and Sigurdsson* [1989] used isopach maps to determine peak values for the first, dominantly buoyant, phase. For the climactic pyroclastic flow phase, *Wilson* [1985] used velocity estimates deduced from field studies together with the total mass of the deposit and obtained a mass discharge rate of 8×10^9 kg s^{-1}. *Bursik and Woods* [1996] used a theoretical model of pyroclastic flow emplacement and obtained a value of 2×10^{10} kg s^{-1}. Water concentration and phenocryst content are estimated to be 4.3 wt % and <5%, respectively [*Dunbar et al.*, 1989]. There were ≈15% lithics in the flow [*Wilson and Walker*, 1985].

2.5. The 1985 Nevado del Ruiz

The relatively short-lived buoyant phase of the Nevado del Ruiz eruption (≈20 mn) generated an atmospheric column which reached an altitude of ≈30 km [*Naranjo et al.*, 1986]. Even for such a small event, the discharge rate estimate derived from lithic isopleths and steady state eruption models is in good agreement with the value obtained from the total deposit volume and eruption duration. The buoyant phase was rapidly followed by pyroclastic flows and surges and hence was close to a transitional regime. The initial amount of water in the magma was 3 wt %, and the phenocrysts content was 40% [*Melson et al.*, 1990]. There were ≈20% lithics in the flow [*Naranjo et al.*, 1986].

2.6. The 1815 Tambora

The Tambora eruption started with a few buoyant phases and switched abruptly to pyroclastic flow and surge generation, indicating column collapse [*Sigurdsson and Carey*, 1989]. This case is particularly interesting as it involves volatile-poor magma, with water concentrations as low as 1.4 wt % in the late surge phase [*Sigurdsson and Carey*, 1989]. The phenocrysts content of the magma was 15%, and there were ≈8% lithics in the flow [*Sigurdsson and Carey*, 1989].

2.7. Minoan, Santorini

The initial phase (phase 1) of the Minoan eruption produced a well-developed fall deposit with few traces of pyroclastic flows or surges [*Sparks and Wilson*, 1989]. We therefore classify the column regime as buoyant. At the end of this phase the eruption underwent a major change of regime which is interpreted as phreatomagmatic. The magma had 6 wt % dissolved water [*Cottrell et al.*, 1999] and 15% phenocrysts [*Druitt et al.*, 1989]. The deposits contain ≈10% lithics [*Pyle*, 1989].

2.8. Fogo A

The deposit of Fogo A is an accumulation of thin fine-grained interstratified layers [*Walker and Croasdale*, 1970], indicating the generation of pyroclastic flows while a buoyant column was developing over the vent. It is therefore classified as transitional. Estimates for the eruptive parameters are 10^8 kg s^{-1} for the peak mass discharge rate [*Carey and Sigurdsson*, 1989], 2.9 wt % for the initial dissolved water concentration, 5% for the phenocryst content [*Gardner et al.*, 1996], and 14% for the amount of lithics [*Walker and Croasdale*, 1970].

2.9. The 1982 El Chichón

The initial phase (A) of the El Chichón eruption was buoyant and had no associated surges, which puts it in the pure buoyant regime. The two subsequent buoyant phases (B and C) were accompanied by surges [*Sigurdsson et al.*, 1987], which puts them in the transitional regime. The initial magma had 6.0 wt % water [*Luhr*, 1990] and 15% phenocrysts [*Sigurdsson et al.*, 1987]. The amount of lithics was large, ≈30% [*Sigurdsson et al.*, 1987].

2.10. Bishop Tuff

The powerful Bishop Tuff eruption has been reevaluated recently by *Wilson and Hildreth* [1997]. The deposit is made of several distinct units but accumulated without detectable breaks. The basal fall layer (F1) appears to be a pure fall deposit with negligible flow units, corresponding to a buoyant regime. Large ignimbrites are found at some intermediate level in the second fall unit (F2). Thereafter, the deposit is of a composite nature, with intercalations of fall and flow components, indicating a transitional regime (F3 to F8). During these phases the amount of water in the magma was nearly constant, with an average value of 5.7 wt % [*Wallace et al.*, 1999]. Toward the end of the eruption, after a short time break (between F8 and F9), eruption resumed with a magma poorer in volatiles, with 4.1 wt % water [*Wallace et al.*, 1999]. Ignimbrite lay-

ers are largely dominant in that late phase, indicating that the eruption was very close to the collapse regime. We have estimated mass discharge rates using the column height estimates of *Wilson and Hildreth* [1997] and the theoretical column models of *Woods* [1988]. The amount of lithics in the deposit is ≈5%, and the percentage of phenocrysts in the magma was ≈10% [*Gardner et al.*, 1991].

2.11. Summary

This overview emphasizes that there is rarely a pure buoyant phase and that pyroclastic flows and surges are very often produced together with a Plinian fall deposit. This indicates that the eruptions were close to collapse conditions in a transitional regime. There are two clear-cut collapse cases at Tambora and Taupo, for which there is no evidence for high atmospheric columns feeding laterally extensive umbrella clouds.

3. Theoretical Models of Volcanic Flows

3.1. Velocity at the Base of the Atmospheric Column

Eruption conditions at the vent depend on the shape of the volcanic conduit. If the conduit has a constant radius, the volcanic mixture is erupted with a sonic velocity and a flow pressure larger than the atmospheric value. In this case, conditions at the base of the atmospheric column depend on the history of decompression above the vent. If the jet decompresses freely, the basal velocity U_f is supersonic at the end of the expansion phase and takes the following value [*Woods and Bower*, 1995]:

$$U_f \approx 0.185\sqrt{n\,RT}, \tag{1}$$

where T is temperature (in K), R is the perfect gas constant, and n is the amount of water in the mixture (in wt %). For an average temperature of 1200 K and taking R=461.5 J kg^{-1} K^{-1} for water, the exit velocity is (in m s^{-1})

$$U_f \approx 138\sqrt{n}. \tag{2}$$

If decompression occurs in a deep and wide crater, the resulting basal velocity is a complex function of eruptive mass flux and crater shape, and its value can cover a wide range, from subsonic to supersonic values. If the driving pressure gradient is lithostatic in the conduit, which requires a specific flaring shape, the volcanic mixture is erupted at atmospheric pressure with a supersonic velocity which is larger than the free decompression value by a factor of ≈2 [*Wilson et al.*, 1980]. For the sake of argument, we will use the free decompression estimate in section 3.2.

3.2. Atmospheric Column Behavior

Many fluid dynamical models of explosive atmospheric column rely on "integral" formulations, in which the problem is reduced to variations in the vertical dimension only and a closure equation is needed for the entrainment of air (see Appendix A). Others rely on more complex sets of two-phase flow equations involving various degrees of simplification and require more elaborate numerical solutions [e.g., *Valentine and Wohletz*, 1989; *Neri and Dobran*, 1994]. These models are sensitive to grid size and closure equations for turbulence over smaller length-scales [*Oberhuber et al.*, 1998]. We know of only one comparison between different models: *Neri and Dobran* [1994] show the conditions for column collapse to be intermediate between the integral results of *Woods* [1988] and *Wilson* [1976]. Integral models are advantageous: They are easy to implement and key hypotheses are readily identified and modified. They do provide satisfactory accounts of different types of analog eruption experiments in the laboratory [*Carey et al.*, 1988; *Woods and Caulfield*, 1992]. They are also consistent with direct observations on several natural eruptions [*Naranjo et al.*, 1986; *Carey et al.*, 1990; *Sparks et al.*, 1997].

Since the early integral model of *Wilson* [1976], new treatments of the dynamics of the lower part of the eruption column, called the "gas thrust" region, have been developed. *Woods* [1988] has proposed a more general theory for turbulent entrainment, as discussed in detail in Appendix A. In this theory the entrainment rate is larger than in the original calculations of *Wilson* [1976] and implies an enlarged domain for the buoyant regime. For the purposes of comparing theoretical predictions with field data it is important to determine the uncertainties involved. For this, we consider several models of entrainment in the atmospheric column. In Appendix A we develop a slightly improved parameterization procedure which leads to results intermediate between those of *Woods* [1988] and *Wilson* [1976]. For the sake of discussion, we shall use both this new model and that of *Woods* [1988].

The threshold velocity separating the buoyant and collapse regimes may be calculated as a function of gas content and basal jet radius (or, equivalently, as a function of mass discharge rate). If the eruption velocity is smaller than this threshold value, the atmospheric column collapses and generates a pyroclastic flow. The threshold velocity increases with decreasing gas content and increasing mass flux. Using the model of Appendix A, values of the threshold velocity V (in m s^{-1}) are close to predictions of

$$V = (3.09 - 0.17\,n)\;M^{1/5}, \tag{3}$$

where M is mass discharge rate in kg s^{-1} and gas content n is in wt %. For n between 0.1 and 7 wt % and M between 10^4 and 10^{10} kg s^{-1}, deviations from this equation are less than ±3%. With the *Woods* [1988] entrainment model the threshold velocity is increased by ≈10%. Considering a maximum range of 0.06-0.12 for the entrainment constant, threshold velocity values are within ±20% of the predictions of (3).

For the purposes of this study the different column regimes are best defined with the usual variables of mass discharge rate and gas content. Assuming free expansion conditions and substituting for the basal velocity (equation (2)) into the threshold velocity equation (3), we obtain the following relationship between threshold mass discharge rate and gas content:

$$M = \left(\frac{138\, n^{1/2}}{3.09 - 0.17\, n} \right)^5 . \qquad (4)$$

Using end-member models for entrainment (see Appendix A), we estimate that the maximum uncertainty on the threshold mass discharge rate is about ±50%.

Figure 1 summarizes theoretical predictions for the eruption regime (buoyant or collapse) and is a revised version of the diagram of *Wilson et al.* [1980]. Figure 1 relies on the amount of magmatic gas carrying the pyroclasts in suspension at the base of the atmospheric column. So far, however, we have only quoted data on the total amount of gas dissolved in the magma prior to eruption. Thus one additional step is required, which is to specify the relationship between these two values of gas content.

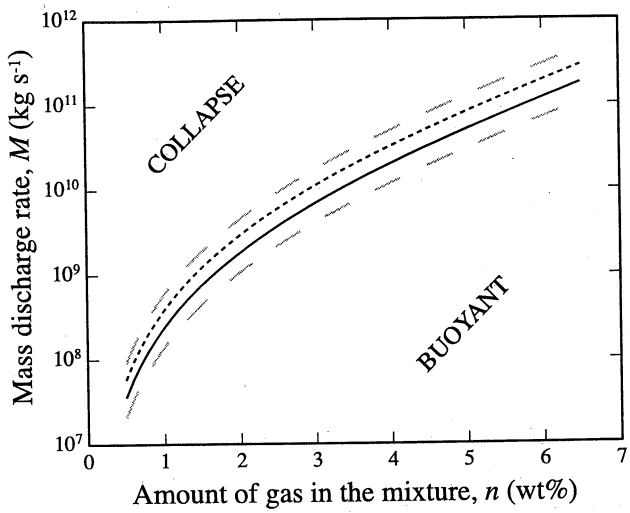

Figure 1. Threshold mass discharge rate for the transition between buoyant and collapse regimes, as a function of gas content in the volcanic mixture (in wt %). Four different curves are given, corresponding to different models for entrainment into the turbulent atmospheric column (see Appendix A). The top dashed curve corresponds to an entrainment constant k=0.12, which leads to an enlarged domain for the buoyant regime. The bottom dashed curve corresponds to k=0.06, which leads to an enlarged domain for the collapse regime. The short dashed and solid curves correspond to the models of *Woods* [1988] and *Kaminski and Jaupart* [1997], respectively. These models lead to intermediate results between the $k = 0.06$ and $k = 0.12$ cases.

4. Comparison Between Model Predictions and Observations

4.1. Ten Eruptions in the Regime Diagram

We use the simple hypothesis that all the magmatic water exsolves and collects into the gas phase which carries the pyroclasts. We then calculate the gas content of the erupting mixture with due consideration for phenocrysts and lithics (Table 1). Finally, we set the velocity at the base of the column to U_f (equation (2)), corresponding to "free expansion" basal conditions. Figure 2 shows the 10 eruptions described above, together with the theoretical prediction for the threshold discharge rate and the associated uncertainty of ±50%.

All eruptions but two (Taupo and Tambora) are well into the buoyant domain. The Tambora and Taupo eruptions are shown as starting in the buoyant domain and ending up at the boundary with the collapse domain. This should correspond to a transitional deposit of interlayered fall and flow units, rather than the pure flow deposit observed. For the eight other eruptions, model predictions are not in agreement with the observations. The Bishop Tuff and Mount St. Helens eruptions, for example, are far from the collapse domain with mass fluxes which are too low by more than one order of magnitude. All the eruptions with transitional characteristics are also located very far from the threshold curve. From these comparisons, it is clear that the simple model of free decompression outside the vent with complete exsolution of the magma is not able to account for all the observations. Furthermore, one may note that the parameters for several eruptions occurring in different regimes (transitional or buoyant) are almost identical. This indicates that other factors must be considered, such as inaccurate data or flaws in the theory.

4.2. Data Accuracy

In order to bring eruption conditions close to the transitional curve, one needs to decrease most estimates of gas content by at least 2 wt % or to increase mass discharge rates by at least one order of magnitude. Are the data biased systematically?

Determinations of mass discharge rate are affected by an uncertainty of about ±50%. This may be demonstrated using the differences between predicted and observed column heights at Mount St. Helens [*Carey et al.*, 1990]. This is also shown by comparing end-member calculations, as for the Minoan deposit, Santorini [*Sparks and Wilson*, 1989], and by comparing independent estimation methods, as at Taupo [*Wilson*, 1985; *Bursik and Woods*, 1996].

The volatile contents of natural magmas may be estimated using melt inclusions within phenocrysts and petrological analyses of coexisting phenocrysts. Both yield similar results [*Cottrell et al.*, 1999] with a typical uncertainty of ≈0.5 wt %. Improvements in experimental techniques have not led to significant changes, as shown by successive studies of the Bishop Tuff [*An-*

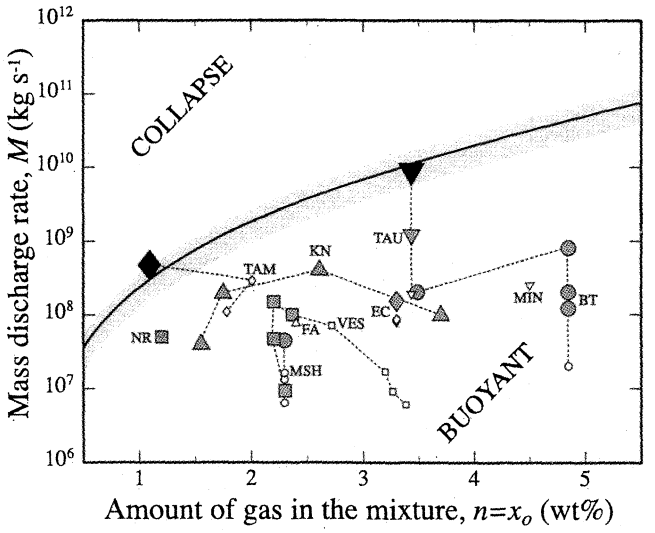

Figure 2. Eruptive conditions of the 10 eruptions of Table 1 in the regime diagram. The threshold mass flux for column collapse is given for the entrainment model of *Kaminski and Jaupart* [1997] with an associated uncertainty of ±50% (shaded area). The small open symbols correspond to eruptions occurring in the buoyant regime, the shaded symbols correspond to eruptions occurring in the transition regime, and the large solid symbols correspond to eruptions occurring in the collapse regime. BT, Bishop Tuff; TAM, Tambora; TAU, Taupo; VES, Vesuvius; NR, Nevado del Ruiz; MIN, Minoan; KN, Katmai-Novarupta; FA, Fogo A; MSH, Mount St. Helens; and EC, El Chichón. Here the Taupo and Tambora eruptions evolve toward transitional conditions, whereas they clearly ended in the collapse regime. All the other eruptions are far from the transition curve, contrary to the observations.

derson et al., 1989; *Dunbar and Hervig*, 1992; *Wallace et al.*, 1999] and of the Minoan eruption, Santorini [*Gardner et al.*, 1996; *Cottrell et al.*, 1999].

One source of error may result from incomplete sampling of an eruption sequence if the magma chamber is stratified in volatile content. This problem is most accute for large eruptions which eject a significant fraction of the chamber contents. When the information was available, each eruptive phase in Table 1 was assigned its proper volatile concentration, including those of the enormous Bishop Tuff, Katmai, and Taupo eruptions. Detailed petrological studies have led *Wallace et al.* [1999, p. 20,120] to conclude that "the mode of emplacement (pumice fall versus pyroclastic flow) is unrelated to preeruptive dissolved volatile contents."

The discrepancy between model predictions and observations may lead one to suspect some systematic overestimation of volatile contents. However, the agreement between independent results from different experimental methods and different laboratories, as well as their levels of uncertainty, does not support this hypothesis. In this context, it is worth remembering that volatile species other than water, such as CO_2, have been neglected in Table 1, implying that the total amount of gas available is, in fact, slightly underestimated.

4.3. Model Uncertainties

To develop a comprehensive flow model accounting for all the processes involved in explosive eruptions is a formidable task. Even the most sophisticated studies of gas-particle turbulent jets fall short of the scale and complexity of true eruption columns [*Ishii et al.*, 1989; *Eaton and Fessler*, 1994; *Oberhuber et al.*, 1998]. However, an "exact" model may not be necessary because the data themselves are not perfectly accurate. In such conditions a fruitful approach is to evaluate the uncertainties associated with the available integral models and to compare them with those of the data.

Uncertainties in the closure equation for entrainment in the dense basal region of an atmospheric column may be responsible for an error of as much as 50% on the threshold mass flux, as shown in section 4.2. Another potential source of error comes from the assumption of a homogeneous mixture, such that gas and suspended pyroclasts are in thermal equilibrium. In reality, the efficacy of heat exchange between these two phases is limited by thermal diffusion through magma, with large fragments shedding only part of their heat [*Woods and Bursik*, 1991; *Kaminski and Jaupart*, 1997]. This reduces the average column buoyancy and hence favors collapse. For most fall and flow deposits, however, the average grain size is quite small [*Woods and Bursik*, 1991; *Kaminski and Jaupart*, 1998], implying that the degree of thermal disequilibrium between gas and pyroclasts is small. According to the calculations by *Woods and Bursik* [1991], for the appropriate values of average grain size, <10% of the magmatic heat is not involved in thermal exchange, and the threshold velocity value for collapse is increased by only a few percent. This may be considered negligible here.

Uncertainties in model predictions and data are of comparable magnitude and too small to explain the discrepancy between theory and observations shown in Figure 2. The fault therefore does not seem to lie with the integral models. As stated in section 3.2, they have been tested succesfully against laboratory experiments and direct observation of eruptive columns. The only option left is to reevaluate the assumptions used to calculate the input parameters for these models.

4.4. Velocity at the Base of the Atmospheric Column

So far, we have assumed that the eruptive jet decompresses freely above the vent, but the situation can be quite different in a crater. Depending on mass discharge rate and crater dimensions, the flow may become subsonic, which may lead to column collapse [*Woods and Bower*, 1995]. However, several arguments suggest that this explanation is not likely for the eruptions of Table 1.

Kaminski and Jaupart [1997] have shown how pumice vesicularity provides constraints on decompression rates and hence eruption velocities. In the Bishop Tuff case they found that eruption velocities must have been supersonic.

The "crater" model really only applies to small eruptions, whereas the 10 eruptions of Table 1 were all quite powerful. The two clear-cut collapse phases are associated with large mass discharge rates in excess of 5×10^8 kg s^{-1}. In such cases, very deep craters would be required to significantly reduce eruption velocities [*Woods and Bower*, 1995]. For example, for the volatile-rich Taupo case the crater would have had to be deeper than 1 km, which seems unrealistic.

Constraints on crater generation are available for two eruptions in our list. At Mount St. Helens in May 1980, a crater was formed in the initial "blast" which destroyed the upper part of the volcanic edifice and did not evolve further. The initial phases had an increasing mass flux and nearly saw a switch to collapse conditions [*Carey et al.*, 1990]. The vent was relatively narrow, and free decompression above it would lead to a jet with a 500-m radius, comparable to the size of the crater [*Woods and Bower*, 1995]. In this case, the flow probably separated from the crater walls and was not affected by them. In the 1912 Katmai-Novarupta eruption, caldera collapse did not affect the vent area, and the crater mouth can be observed in the field. It has a diameter of $\approx$2 km at the surface, and its depth extent is unknown [*Hildreth*, 1987]. Such a wide crater probably had a small effect on expansion conditions above the vent.

5. Gas Content of the Eruptive Mixture

During ascent in a volcanic conduit, magma degassing depends on the kinetics of several complex processes, and only maximum efficiency can lead to complete exsolution. To evaluate the effective gas content of the mixture, one must look at fragmentation and pyroclast generation in detail.

Bubbly magma undergoes fragmentation under conditions which remain poorly understood. A discussion of the various models proposed [*Sparks*, 1978; *Webb and Dingwell*, 1990; *Gardner et al.*, 1996; *Papale*, 1999] is outside the scope of this paper, and we use the simplest criterion for fragmentation, such that the volume fraction of gas in the mixture exceeds a critical threshold of 70%. This value is close the predictions of the relaxation model of *Webb and Dingwell* [1990] for the viscous magmas involved in the eruptions of Table 1 [*Papale*, 1999]. Using the solubility law and the equation of state for water, a straightforward calculation then leads to the fragmentation pressure and the mass fraction of gas at fragmentation, x_f [*Wilson et al.*, 1980]. However, this specifies the total amount of gas present, which is not sufficient. There is an "internal" gas phase within the vesicular magma fragments and an "external" continuous gas phase carrying pyroclasts in suspension. We denote by x_g the mass fraction of this external gas phase.

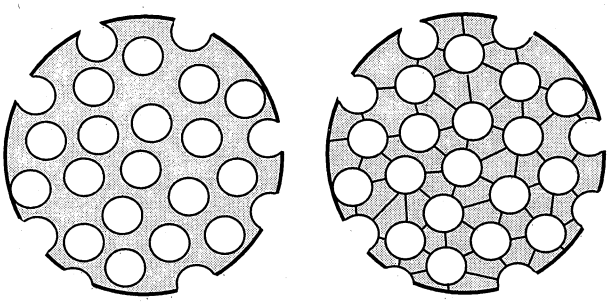

Figure 3. Two end-members for the amount of gas available in the mixture. If the bubbles form an interconnected network, all the gas dissolved in magma is available. If the bubbles are trapped inside the fragment, only the gas released by the fragmentation process is available.

One must determine what happens to gas bubbles within magma fragments after fragmentation, as the flow goes through the final phase of ascent and decompression (Figure 3). As shown by *Kaminski and Jaupart* [1997], the decompression rate is so large that isolated gas bubbles within a pyroclast cannot expand rapidly enough to keep up with the external flow pressure. We do know that bubbles become interconnected at some stage because most natural pumices are permable when collected on the ground. If this occurs in the conduit, below the vent, pressure differences between the internal and external gas phases remain small at all times and magma degassing can proceed to near completion. In this case, one has $x_g = x_o$ (amount of continuous gas phase equal to total amount of dissolved volatiles). However, this is not consistent with analyses of matrix glass from pumice samples, which provide evidence that magma retains significant amount of volatiles in solution [*Taylor*, 1991; *Westrich et al.*, 1988; *Blank et al.*, 1994]. In an earlier study, using a physical model for the expansion of vesicular magma fragments, we have argued that bubble interconnection occurs late in the eruption sequence, upon quenching in the upper part of the atmospheric column [*Kaminski and Jaupart*, 1997]. Laboratory studies on the behavior of vesicular magma demontrate that quenching does indeed generates permeable pumice samples [*Mungall et al.*, 1996]. A realistic hypothesis is thus that the internal gas phase remains isolated from the external one.

Fragmentation can be regarded as generating interfaces through bubbly magma, which separate individual fragments (Figure 4). Bubbles intersected by these interfaces release their gas, which collects into the continuous external phase. Bubbles which are not intersected remain trapped inside the fragments and do not release their gas. Thus they form an independent internal gas phase. Further volatile exsolution and internal

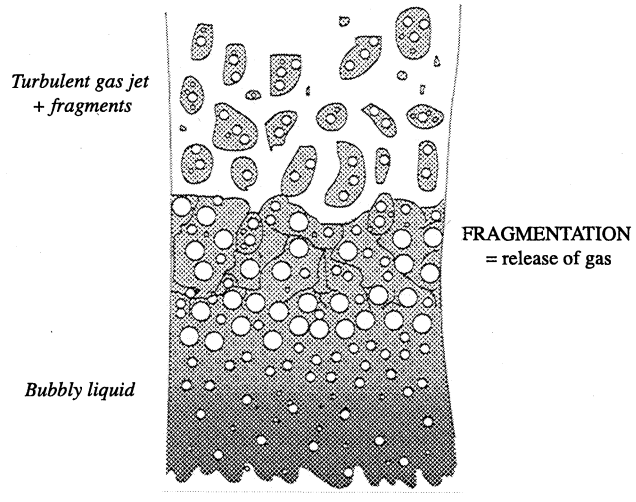

Figure 4. Fragmentation sequence in an explosive eruption. Fragmentation generates interfaces through the bubbly magma and separates individual fragments. Only the bubbles intersected by these interfaces release their gas to form a continuous external phase.

gas expansion may occur during decompression before exit into the atmosphere, but this gas remains trapped within the fragments. Thus the mass of external gas remains constant and equal to the amount at fragmentation. *Kaminski and Jaupart* [1998] have demonstrated that for a mean bubble radius b the fraction of gas released by the formation of a spherical fragment of size r is

$$\frac{x_g}{x_f} = 3\frac{b}{r}. \tag{5}$$

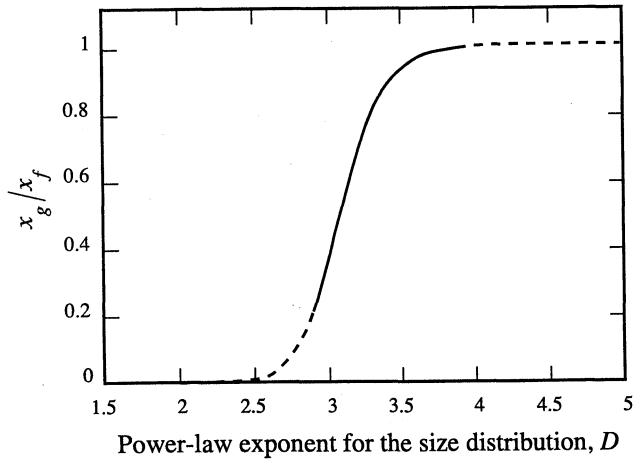

Figure 5. Fraction of exsolved gas released at fragmentation as a function of the exponent of the power law. For exponents larger than 3, the population of pyroclasts consists mainly of ash particlees and a large amount of gas is released. For exponent values smaller than 3, pyroclasts are large, and the gas content of the erupted mixture is small. Values of D in fall and flow deposits are between 2.9 and 3.9 [*Kaminski and Jaupart*, 1998]. Portions of the curve which fall outside this range have been dashed.

Only those fragments that are smaller than the bubbles cannot retain any gas. For typical bubble sizes (<1 mm), this applies solely to ash particles, and hence the amount of gas released at fragmentation depends on the size distribution of pyroclasts.

The size distribution of pyroclastic populations follows a power law [*Kaminski and Jaupart*, 1998], such that $N(R \geq r)$, the number of fragments larger than r is given by

$$N(R \geq r) \propto r^{-D}, \tag{6}$$

where D is a positive exponent. The fraction of gas released at fragmentation may be calculated as a function of D and as a function of the bubble size distribution and the smallest fragment size. As discussed by *Kaminski and Jaupart* [1998], provided that bubble and fragment sizes are taken within realistic ranges, the results are not very sensitive to the exact values chosen. Figure 5 shows the fraction of gas released at fragmentation and emphasizes that the limit $x_g = x_f$ is not valid for values of D less than 3.5. No pyroclastic flow population meets this criterion, and very few fall populations do [*Kaminski and Jaupart*, 1998]. This argument demonstrates that the amount of continuous magmatic gas may be much smaller than has hitherto been assumed.

6. A Revised Regime Diagram

We have argued that crater formation did not affect the powerful eruptions of Table 1 and hence propose that in a majority of cases, free expansion conditions provide the best approximation to real eruptive conditions. In the case of imperfect fragmentation the threshold mass flux for column collapse must be evaluated in

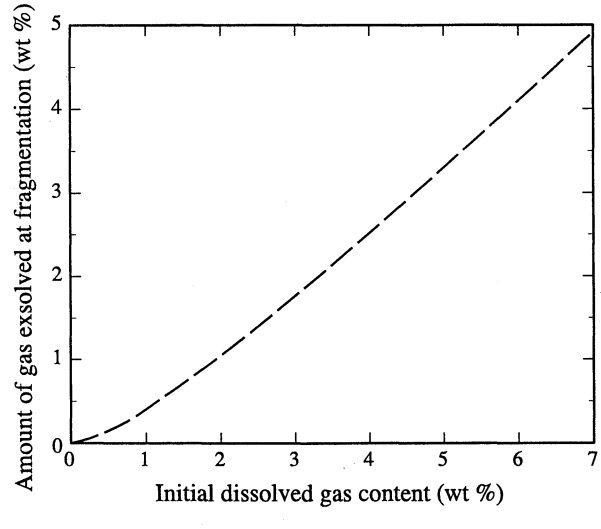

Figure 6. Amount of exsolved gas at fragmentation as a function of the total amount of volatiles initially dissolved. The curve has been calculated using the solubility law for water in rhyolitic magma. The threshold value for vesicularity at fragmentation has been set to 70%.

two steps. For an initial total amount of gas dissolved in the magma, n_o, one may first account for the presence of phenocrysts and lithics to obtain x_o the total amount of gas in the mixture (liquid+phenocrysts+lithics+gas). One then calculates x_f the amount of gas exsolved at fragmentation for a given threshold vesicularity, using a solubility law (Figure 6). Once x_f is known, x_g may be calculated as a function of D, the exponent of the grain size distribution (Figure 5). The threshold mass flux is then obtained by setting $n = x_g$ in(4).

Changing the amount of gas in the mixture changes the threshold mass flux for column collapse but does not affect significantly calculations for buoyant columns in the Plinian regime. The reason for this is that at high altitudes the gas phase is dominated by entrained atmospheric air [*Woods*, 1995]. Thus mass discharge rate estimates obtained from the characteristics of fall deposits are reliable and can be used to test the new threshold condition.

6.1. Taupo Eruption

The Taupo eruption is the only one for which all the required data are available, including the grain-size distribution [*Kaminski and Jaupart*, 1998]. It also reached the largest mass discharge rate known, for which crater formation is least likely to have an impact on shallow decompression conditions. Thus, one expects that the free expansion model is close to the true eruptive conditions. We use D=3.3 as appropriate for the pyroclast population in this eruption [*Kaminski and Jaupart*, 1998], which corresponds to $x_g = 0.8\,x_f$ (Figure 5). At Taupo the total initial amount of gas dissolved in the magma was n_o=4.3 wt % (Table 1). Taking into account the phenocrysts and lithics, the amount of gas in the mixture (liquid+phenocrysts+lithics+gas) was x_o = 3.4 wt %. From Figure 6 the amount of water exsolved at fragmentation was x_f = 2.2 wt %, which leads to x_g = 1.8 wt %. The amount of gas in the flow at the vent was thus $n = x_g$ = 1.8 wt %.

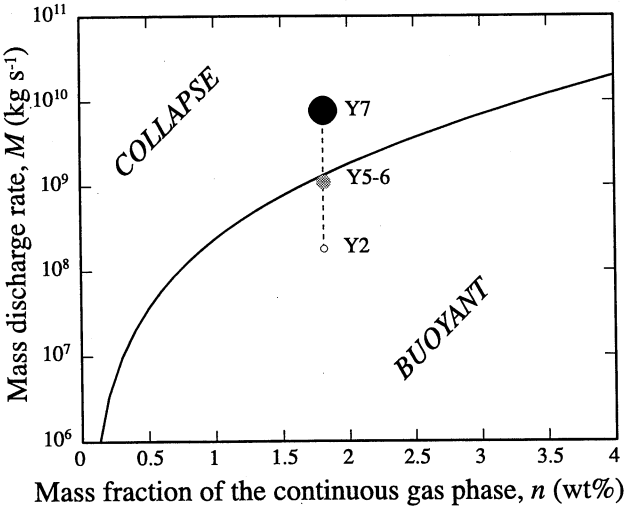

Figure 7. Eruptive conditions for the Taupo eruption if the mass fraction of the continuous gas phase in the mixture is corrected for the size distribution of pyroclasts (data from *Kaminski and Jaupart* [1998]). The model predicts a purely buoyant first phase, a second phase evolving toward the transitional regime, and a final phase marked by complete collapse, in agreement with field observations.

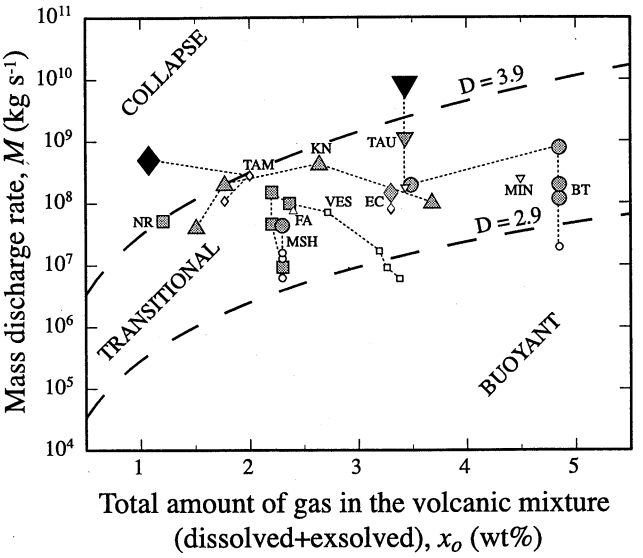

Figure 8. The ten eruptions of Table 1 in the new regime diagram (see Figure 2 legend). The threshold mass flux is calculated for a vesicularity of 70% at fragmentation, and for two extreme grain size distributions (corresponding to power law exponents D = 2.9 and D = 3.9). The two curves define a transitional region, in which the column is likely to be marginally stable. In this region the column behavior is highly sensitive to the amount of volatiles, the mass discharge rate, and the grain-size distribution of pyroclasts.

Figure 7 shows the evolution for the Taupo eruption, with the new gas content estimate. The mass discharge rate for the early Hatepe Plinian phase (Y2) still places this eruption in the buoyant domain. However, the Taupo pumice deposit (Y5) is now very close to the transition curve, which suggests a transitional regime with the simultaneous generation of fall and flow deposits. The climactic phase is well into the collapse domain and hence is predicted to be in the pure pyroclastic flow regime. Such an eruption sequence is entirely consistent with the observations summarized in section 2.4.

6.2. Overview

The grain size distributions for the other eruptions of Table 1 are not known. *Kaminski and Jaupart* [1998] have shown that values of the power law exponent of many pyroclast populations vary from 2.9 to 3.9. Using a value for D allows us to draw a regime diagram using the total amount of gas available, x_o (which accounts for lithics and phenocrysts). The value of 2.9 leads to

the smallest gas contents ($x_g = 0.16\,x_f$) and thus provides the most favorable conditions for column collapse, whereas the value of 3.9 corresponds to the most favorable conditions for a buoyant column ($x_g = 0.99\,x_f$). In Figure 8 the domain bounded by the two transition curves for the two extreme values of the exponent defines a transitional domain. According to the model, all the eruptions of Table 1 should be in that domain, which is indeed the case (Figure 8). The last phase of the Tambora eruption now lies well within the collapse domain, which is now consistent with the field observations.

In many cases, the eruptive conditions are close to the buoyant/collapse transition region. Thus small changes of the size distribution of pyroclasts, which lead to important changes of gas content (Figure 5), may determine which eruption regime ensues. Two eruptions with the same mass flux and the same initial amount of gas can occur in different regimes if their grain size distributions are different. On the whole, eruptions in the collapse or transitional regimes should be associated with lower external gas contents than those in the buoyant regime, which may be achieved simply by a coarser fragmentation sequence. One therefore expects that the power law exponents of fall deposit populations are systematically larger than those of flow deposit populations. This is indeed true [*Kaminski and Jaupart*, 1998].

7. Discussion

In explosive eruptions a key process is the interconnection of bubbles within pyroclasts. Many authors consider that this happens early in the conduit and that volatile exsolution proceeds to completion [e.g., *Cashman and Mangan*, 1994]. We have given above several lines of evidence which contradict this. Some authors have recognized this and have considered values of gas content which are smaller than the initial volatile concentration of magma. For example, in his study of the 1350 A.D. North Mono crater eruptions, *Bursik* [1993] used volatile concentrations preserved in obsidian clasts [*Newman et al.*, 1988] to calculate directly the exsolved gas content of each eruptive phase. However, one must also account for the internal gas phase within vesicular pyroclasts.

Plinian eruptions are well accounted for by available models because the gas phase at high altitude is predominantly made of entrained atmospheric air. In contrast, the conditions for column collapse depend critically on the amount of magmatic gas and hence on the details of flow and fragmentation in the volcanic conduit. They also depend on the dynamics of entrainment in the lower parts of atmospheric eruption columns, where the erupted mixture is denser than surrounding air. Pyroclastic flow eruptions therefore provide stringent constraints on processes occurring below the vent and at small altitudes above the vent.

We have emphasized that the size distribution of pyroclasts plays an important role in the eruption process. It should also be noted that pyroclasts carry most of the momentum and heat of the eruptive jet. Momentum and heat transfer from the fragments to the continuous gas phase is a function of particle size. *Woods and Bursik* [1991] have shown that coarse grain-size distributions are in favor of column collapse because they act to decrease the efficacy of thermal exchange between gas and suspended particles. We have argued that such distributions are also in favor of column collapse because they act to decrease the amount of external gas in the mixture. Thus the two effects reinforce one another. Therefore the grain-size distribution of pyroclasts is a key variable and must be included in a realistic eruption model.

8. Conclusion

In this paper, we have compiled data and field observations from 10 explosive eruptions in order to test fluid dynamical models of eruptive column behavior. Model predictions are in agreement with observations only if one accounts for the amount of gas trapped in gas bubbles within pyroclasts. We present a new regime diagram for the transition between buoyant and collapsing column based on the effective amount of continuous gas phase in the mixture. We have shown that the grain-size distribution of pyroclasts plays a key role in eruption dynamics because it controls the amount of gas released at fragmentation. It also controls the transfer of heat and momentum between gas phase and magma fragments and hence is a key variable which must be included in eruption models. Our arguments illustrate the many different ways in which small objects such as pyroclasts and bubbles within pyroclasts affect large-scale destructive flows.

Appendix A: Entrainment in the Basal Region of Atmospheric Eruption Columns

Here we recapitulate and complete a few points already developed by *Woods* [1988, 1995] and *Kaminski and Jaupart* [1997]. Predicting column collapse depends critically on the rate at which the volcanic mixture becomes lighter as it mixes with surrounding air. In integral flow models this appears in the mass conservation equation written as

$$\frac{\mathrm{d}}{\mathrm{d}z}\left(\rho U L^2\right) = 2\,\rho_a\,\epsilon L, \tag{A1}$$

where ρ is the average jet density at height z above ground, ρ_a is the density of surrounding air, U is the mean vertical velocity, L is the equivalent jet radius, and ϵ is the entrainment rate.

All models of this sort depend on the relationship between the entrainment rate ϵ and the bulk flow charac-

teristics. From dimensional arguments, one has $\epsilon = kU$, which defines the "entrainment constant" k, and the various hypotheses may be discussed with this constant. For an eruption model one must consider three different issues. One is that buoyant plumes, single-phase turbulent jets, and particle-laden jets have different dynamics [*Hinze*, 1975; *Chung and Troutt*, 1988; *Papanicolaou and List*, 1988]. One other issue is that the flow velocity structure, as defined, for example, by the radial profile of vertical velocity, changes between the vent and the fully developed region at some distance. Finally, the density difference between the jet and its surroundings may be large, which affects the efficacy of entrainment.

In the approximation that ρ is very close to ρ_a, there is a difference between the "basal thrust" and buoyant parts of a column. In the former, close to the vent, the flow is propelled by its momentum and behaves as a jet, such that $k \approx 0.06$ [*Papanicolaou and List*, 1988]. Farther from the vent, the column may become buoyant, in which case $k \approx 0.09$ [*Papanicolaou and List*, 1988]. With dense particles, laboratory experiments suggest that $k \approx 0.12$ [*Carey et al.*, 1988; *Ernst et al.*, 1996]. *Wilson et al.* [1980] used $k = 0.09$, which is strictly valid only for buoyant plumes.

In a volcanic conduit, flow is in fully developed turbulence with a top-hat radial profile of vertical velocity. Above the vent, in the atmospheric column, this profile gradually changes toward a bell shape as entrainment eddies develop at the edge of the jet. Radial profiles of velocity, temperature, and density are defined by the axis ($r = 0$) and by a dimensionless shape function $f(r)$, such that $f(0) = 1$ and $f(r)$ tends to zero as r goes to infinity. We assume that this dimensionless "shape" function is the same for the three variables, which is a valid approximation [*Turner*, 1979; *Woods*, 1988, 1995]. For example, the mass flux is written as

$$\begin{aligned} \rho U \pi L^2 &= \int_0^\infty \rho(r) U_M f(r) 2\pi r \mathrm{d}r \\ &= \int_0^\infty \left[\rho_a + \Delta\rho_M f(r)\right] U_M f(r) 2\pi r \mathrm{d}r, \end{aligned} \quad \text{(A2)}$$

where $\Delta\rho = \rho - \rho_a$ is the excess density of the mixture relative to ambient air and $\Delta\rho_M = \rho_M - \rho_a$.

Woods [1988] has extended Prandtl's original theory for jets to allow for density differences between the jet and its surroundings. We rewrite the entrainment equation of *Woods* [1988] in its general form:

$$k = \frac{1}{2}\lambda \left(\frac{U_M}{U}\right)^2 \left(\frac{\rho}{\rho_a}\right)^{1/2}, \quad \text{(A3)}$$

where constant λ takes the value of $1/8 = 0.125$, as determined from experimental data on single-phase turbulent jets [*Prandtl*, 1954; *Hinze*, 1975]. This introduces two factors: one is the radial profile, which appears through ratio U_M/U, and the other is the density ratio. We use the following form for the shape function $f(r)$:

$$f(r,z) = \exp\left[-\left(\frac{r}{\delta(z)}\right)^n\right], \quad \text{(A4)}$$

where $\delta(z)$ provides a measure of column width at height z. At the vent the top-hat velocity profile is described by a large value of n. In this case, $U_M = U$, and hence $k = 0.06\sqrt{\rho/\rho_a}$, or $k \approx 0.06$ for $\rho \approx \rho_a$, as appropriate for most experiments. For a particle-laden jet in the self-similar fully developed region, n takes a value of ≈ 4 [*Chung and Troutt*, 1988], and $U_M = \sqrt{2}U$. Thus $k = 0.125\sqrt{\rho/\rho_a}$, or $k \approx 0.12$ for $\rho \approx \rho_a$, which is consistent with the experimental results of *Carey et al.* [1988] and *Ernst et al.* [1996].

The conservation equations are

$$\frac{\mathrm{d}}{\mathrm{d}z}\left(\rho U L^2\right) = 2\,\rho_a\,\epsilon L, \quad \text{(A5)}$$

$$\frac{\mathrm{d}}{\mathrm{d}z}\left(\rho U^2 L^2\right) = g\left(\rho_a - \rho\right) L^2, \quad \text{(A6)}$$

$$\begin{aligned} \frac{\mathrm{d}}{\mathrm{d}z}\left(\rho C_p \theta U L^2\right) &= -\rho_a U L^2 g \\ &+ \left(C_a T + \frac{U^2}{2}\right)\frac{\mathrm{d}}{\mathrm{d}z}\left(\rho U L^2\right), \end{aligned} \quad \text{(A7)}$$

where θ is the average jet temperature, C_p is the heat capacity for the mixture, T is the atmospheric temperature, C_a is the atmospheric heat capacity, and g is the acceleration of gravity. We do not allow for the settling of particles, and the mass flux of pyroclasts is conserved. We carry out calculations using the above entrainment law and allowing the shape function $f(r)$ to vary from a top-hat profile ($n \gg 1$) at the vent, to $n = 4$, which is valid for particle-laden jets. A variable exponent introduces an additional unknown, and a fourth equation is needed. At small heights above the vent, entrainment only affects the outer regions of the jet and does not reach into the core region. At the centerline, temperature therefore evolves by adiabatic decompression only, and the mass fraction of fragments remains constant. The equation for the centerline temperature θ_M is

$$\frac{\mathrm{d}\theta_M}{\mathrm{d}z} = -\frac{\rho_a}{\rho}\frac{g}{C_p}. \quad \text{(A8)}$$

The equations for the fluxes of mass, momentum, and enthalpy are solved exactly as by *Woods* [1988], and we add the centerline temperature. Thus we determine the values of ρ, U, L, θ, and θ_M at all heights. Using a straightforward change of variables in the integrals, we then write

$$\rho U L^2 = 2U_M \delta^2 I\left(\rho_a + \Delta\rho_M 2^{-2/n}\right), \quad \text{(A9)}$$

$$\rho U^2 L^2 = 2U_M^2 \delta^2 I\left(\rho_a 2^{-2/n} + \Delta\rho_M 3^{-2/n}\right), \quad \text{(A10)}$$

$$\rho U \theta L^2 = 2U_M \theta_M \delta^2 I\left(\rho_a 2^{-2/n} + \Delta\rho_M 3^{-2/n}\right), \quad \text{(A11)}$$

where I is

$$I = \int_0^\infty r \exp(-r^n)\mathrm{d}r. \quad \text{(A12)}$$

From (A9)-(A11), we obtain

$$\frac{\theta}{\theta_M} = \frac{U}{U_M}, \quad \text{(A13)}$$

$$\frac{U}{U_M} = \frac{\Delta\rho_M 3^{-2/n} + \rho_a 2^{-2/n}}{\Delta\rho_M 2^{-2/n} + \rho_a}. \quad \text{(A14)}$$

Ratio θ/θ_M is known because θ and θ_M are both known and $\Delta\rho_M$ is given as a function of temperature and pyroclast content [see *Woods*, 1988]). The value of n is then obtained as the solution of (A14). Exponent n is left to change until it reaches the value of 4 at some height H. The value of H is not assumed and is an output of the model. At that height, turbulence is fully developed and the centerline becomes affected by mixing with colder atmospheric air. For $z \geq H$, therefore, (A8) is no longer valid and n is kept at the value of 4, as appropriate for particle-laden jets [*Chung and Troutt*, 1988]. At greater heights in the atmosphere the concentration of particles eventually becomes small, and the eruption column may develop into a buoyant plume, for which $n \approx 2$ [*Turner*, 1979]. By definition, column collapse does not occur in the buoyant region, and hence there is no need to provide a model for the transition from $n = 4$ to $n = 2$. We determine the conditions for which dense jets reach zero vertical velocity, which corresponds to column collapse.

For the purposes of comparison, we have also taken the entrainment law used by *Woods* [1988], i.e.,

$$k = 0.09 \left(\frac{\rho}{\rho_a}\right)^{1/2}. \quad \text{(A15)}$$

With (A15) the rate of entrainment is larger than in our model at small heights and smaller than in our model at greater heights. The end result is that the quantitative predictions are close to those of our model. We have also considered end-member cases with constant values of the entrainment parameter k set at the minimum value of 0.06 and the maximum value of 0.12 (Figure 1).

Acknowledgments. The authors thank Steve Sparks for fruitful comments on a previous version of the manuscript and acknowledge the constructive input of Steve Carey, Marcus Bursik, and an anonymous associate editor.

References

Anderson, D. J., S. Newman, S. N. Williams, T. H. Druitt, C. Skirius, and E. Stolper, H_2, CO_2, Cl and gas in Plinian and ash-flow bishop rhyolite, *Geology*, *17*, 714–726, 1989.

Blank, J. G., J. E. Gardner, and C. Jaupart, Degassing and fragmentation histories of erupted magma: Evidence from matrix glass in pumice, *EOS Trans. AGU, 75* (44), Fall Meet. Supp., 719, 1994.

Bursik, M. I., Subplinian eruption mechanisms inferred from volatile and clast dispersal data, *J. Volcanol. Geotherm. Res.*, *57*, 57–70, 1993.

Bursik, M. I., and A. W. Woods, The dynamics and thermodynamics of large ash flows, *Bull. Volcanol.*, *58*, 175–193, 1996.

Carey, S. N., and H. Sigurdsson, Influence of particle aggregation on deposition of distal tephra from the May 18, 1980, eruption of Mount St. Helens volcano, *J. Geophys. Res.*, *87*, 7061–7072, 1982.

Carey, S. N., and H. Sigurdsson, Temporal variations in eruption column height and magma discharge rate during the 79 AD eruption of Vesuvius, *Geol. Soc. Am. Bull.*, *99*, 303–314, 1987.

Carey, S. N., and H. Sigurdsson, The intensity of Plinian eruptions, *Bull. Volcanol.*, *51*, 28–40, 1989.

Carey, S. N., H. Sigurdsson, and R. S. J. Sparks, Experimental studies of particle-laden plumes, *J. Geophys. Res.*, *93*, 15,314–15,328, 1988.

Carey, S. N., H. Sigurdsson, J. E. Gardner, and W. Criswell, Variations in column height and magma discharge during the May 18, 1980 eruption of Mount St. Helens, *J. Volcanol. Geotherm. Res.*, *43*, 99–112, 1990.

Cashman, K. V., and M. T. Mangan, Physical aspects of magmatic degassing, II, Constraints on vesiculation processes from textural studies of eruptive products, in *Volatiles in Magmas, Rev. Min.*, vol. 30, edited by M. R. Carroll and J. R. Holloway, pp. 447–478, Mineral. Soc. of Am., Washington D. C., 1994.

Chung, J. N., and T. R. Troutt, Simulation of particle dispersion in an axisymmetric jet, *J. Fluid Mech.*, *186*, 199–222, 1988.

Cottrell, E., J. E. Gardner, and M. J. Rutherford, Petrologic and experimental evidence for the movement and heating of the pre-eruptive Minoan rhyodacite (Santorini, Greece), *Contrib. Mineral. Petrol.*, *135*, 315–331, 1999.

Criswell, W., Chronology and pyroclastic stratigraphy of the May 18, 1980, eruption of Mount St. Helens, Washington, *J. Geophys. Res.*, *92*, 10,237–10,266, 1987.

Druitt, T. H., R. A. Mellors, D. M. Pyle, and R. S. J. Sparks, Explosive volcanism on Santorini, Greece, *Geol. Mag.*, *126*, 95–126, 1989.

Dunbar, N. W., and R. L. Hervig, Petrogenesis and volatile stratigraphy of the bishop tuff: Evidence from melt inclusion analysis, *J. Geophys. Res.*, *97*, 15,129–15,150, 1992.

Dunbar, N. W., P. R. Kyle, and C. J. N. Wilson, Evidence from limited zonation in silicic magma systems, Taupo volcanic zone, New Zealand, *Geology*, *17*, 234–236, 1989.

Eaton, J. K., and J. R. Fessler, Preferential concentration of particles by turbulence, *Int. J. Multiphase Flow*, *20*, 169–209, 1994.

Ernst, G. G. J., R. S. J. Sparks, S. N. Carey, and M. Bursik, Sedimentation from turbulent jets and plumes, *J. Geophys. Res.*, *101*, 5575–5589, 1996.

Fierstein, J., and W. Hildreth, The plinian eruption of 1912 at Novarupta, Katmai National Park, Alaska, *Bull. Volcanol.*, *54*, 646–684, 1992.

Gardner, J. E., H. Sigurdsson, and S. N. Carey, Eruption dynamics and magma withdrawal during the plinian phase of the Bishop Tuff eruption, Long Valley Caldera, *J. Geophys. Res.*, *96*, 8097–8111, 1991.

Gardner, J. E., R. M. E. Thomas, C. Jaupart, and S. Tait, Fragmentation of magma during plinian volcanic eruptions, *Bull. Volcanol.*, *58*, 144–162, 1996.

Hildreth, W., New perspectives on the eruption of 1912 in the Valley of Ten Thousand Smokes, Katmai National Park, Alaska, *Bull. Volcanol.*, *49*, 680–693, 1987.

Hildreth, W., The timing of caldera collapse at Mount Katmai in response to magma withdrawal toward Novarupta, *Geophys. Res. Lett.*, *18*, 1541–1544, 1991.

Hinze, J. O., *Turbulence*, 2nd ed., McGraw-Hill, New York, 1975.

Ishii, R., Y. Umeda, and M. Yuhi, Numerical analysis of gas-particle two phase flows, *J. Fluid Mech.*, *203*, 475–515, 1989.

Kaminski, É., and C. Jaupart, The expansion and quench-

ing of vesicular magma fragments in plinian eruptions, *J. Geophys. Res.*, *102*, 12,187–12,203, 1997.

Kaminski, É., and C. Jaupart, The size distribution of pyroclasts and the fragmentation sequence in explosive volcanic eruptions, *J. Geophys. Res.*, *103*, 29,759–29,779, 1998.

Luhr, J. F., Experimental phase relations of water and sulfur-saturated arc magmas and the 1982 eruptions of El Chichón volcano, *J. Petrol.*, *31*, 1071–1114, 1990.

Melson, W. G., J. F. Allan, D. R. Jerez, J. Nelen, M. L. Calvache, S. N. Williams, J. Fournelle, and M. Perfit, Water contents, temperatures and diversity of the magmas of the catastrophic eruption of Nevado del Ruiz, Colombia, November 13, 1985, *J. Volcanol. Geotherm. Res.*, *41*, 97–126, 1990.

Mungall, E. J., N. S. Bagdassarov, C. Romano, and D. B. Dingwell, Numerical modelling of stress generation and microfracturing of vesicle walls in glassy rocks, *J. Volcanol. Geotherm. Res.*, *73*, 33–46, 1996.

Naranjo, J. L., H. Sigurdsson, S. N. Carey, and W. Fritz, Eruption of Nevado del Ruiz volcano, Colombia, on 13 November 1985: Tephra fall and lahars, *Science*, *233*, 961–963, 1986.

Neri, A., and F. Dobran, Influence of eruption parameters on the thermofluid dynamics of collapsing volcanic columns, *J. Geophys. Res.*, *99*, 11,833–11,857, 1994.

Newman, S., S. Epstein, and E. Stopler, Water, carbon dioxyde and hydrogen isotopes in glasses from the ca. 1340 A.D. eruption of the Mono Craters, California: Constraints on degassing phenomena and initial volatile content, *J. Volcanol. Geotherm. Res.*, *35*, 75–96, 1988.

Oberhuber, J. M., M. Herzog, H. F. Grant, and K. Schwanke, Volcanic plume simulation on large scales, *J. Volcanol. Geotherm. Res.*, *87*, 29–53, 1998.

Papale, P., Strain-induced fragmentation in explosive eruptions, *Nature*, *397*, 425–428, 1999.

Papanicolaou, P. N., and E. J. List, Investigations of round vertical turbulent buoyant jets, *J. Fluid Mech.*, *195*, 341–391, 1988.

Prandtl, L., *Essentials of Fluid Dynamics*, Blackie, Glasgow, 1954.

Pyle, D. M., New estimates for the volume of the Minoan eruption, in *Thera and the Aegean World III*, vol. 2, pp. 113–121, Thera Found., London, 1989.

Rutherford, M., H. Sigurdsson, S. N. Carey, and A. Davis, The May 18, 1980, eruption of Mount St. Helens, 1, Melt composition and experimental phase equilibria, *J. Geophys. Res.*, *90*, 2929–2947, 1985.

Sigurdsson, H., and S. N. Carey, Plinian and co-ignimbrite tephra fall form the 1815 eruption of Tambora volcano, *Bull. Volcanol.*, *51*, 243–270, 1989.

Sigurdsson, H., S. N. Carey, W. Cornell, and T. Pescatore, The eruption of Vesuvius in A.D. 79, *Nat. Geograph. Res.*, *1*, 332–387, 1985.

Sigurdsson, H., S. N. Carey, and R. V. Fisher, The 1982 eruption of El Chichón volcano, Mexico, 3, Physical properties of pyroclastic surges, *Bull. Volcanol.*, *49*, 467–488, 1987.

Sigurdsson, H., W. Cornell, and S. N. Carey, Influence of magma withdrawal on compositional gradients during the AD 79 Vesuvius eruption, *Nature*, *345*, 519–521, 1990.

Sparks, R. S. J., The dynamics of bubble formation and growth in magmas — A review and analysis, *J. Volcanol. Geotherm. Res.*, *3*, 1–37, 1978.

Sparks, R. S. J., and C. J. N. Wilson, The Minoan deposits: A review of their characteristics and interpretation, in *Thera and the Aegean World III*, vol. 1, pp. 95–104, Thera Found., London, 1989.

Sparks, R. S. J., and L. Wilson, Model for the formation of ignimbrite by gravitational column collapse, *J. Geol. Soc.*, *132*, 441–452, 1976.

Sparks, R. S. J., M. I. Bursik, S. N. Carey, J. S. Gilbert, L. S. Claze, H. Sigurdsson, and A. W. Woods, *Volcanic Plumes*, John Wiley, New York, 1997.

Taylor, B. E., Degassing of obsidian dome rhyolite, Inyo volcanic chain, California, in *Stable Isotope Geochemistry: A Tribute to Samuel Epstein*, edited by H. P. Jr. Taylor, J. R. O'Neil, and I. R. Kaplan, *Spec. Pub. Geochem. Soc.*, *3*, pp. 339–353, 1991.

Turner, J. S., *Buoyancy Effects in Fluids*, Cambridge Univ. Press, New York, 1979.

Valentine, G. A., and K. H. Wohletz, Numerical models of Plinian eruption columns, *J. Volcanol. Geotherm. Res.*, *94*, 1867–1887, 1989.

Walker, G. P. L., and R. Croasdale, Two Plinian type eruptions in the Azores, *J. Geol. Soc.*, *127*, 17–55, 1970.

Wallace, P. J., A. T. Anderson, and A. M. Davis, Gradients in H_2O, CO_2, and exsolved gas in a large-volume silicic magma system: Interpreting the record preserved in melt inclusions from the Bishop Tuff, *J. Geophys. Res.*, *104*, 20,097–20,122, 1999.

Webb, S. L., and D. B. Dingwell, Non-Newtonian rheology of igneous melts at high stresses and strain-rates: Experimental results for rhyolite, andesite, basalt, and nephelinite, *J. Geophys. Res.*, *95*, 15,695–15,701, 1990.

Westrich, H. R., H. W. Stockman, and J. C. Eichelberger, Degassing of rhyolitic magma during ascent and emplacement, *J. Geophys. Res.*, *93*, 6503–6511, 1988.

Westrich, H. R., J. C. Eichelberger, and R. L. Hervig, Degassing of the 1912 Katmai magmas, *Geophys. Res. Lett.*, *18*, 1561–1564, 1991.

Wilson, C. J. N., The Taupo eruption, New Zealand, II, The Taupo ignimbrite, *Philos. Trans. R. Soc. London Ser. A*, *314*, 229–310, 1985.

Wilson, C. J. N., Stratigraphy, chronology, styles and dynamics of the late Quaternary eruptions from Taupo volcano, New Zealand, *Philos. Trans. R. Soc. London Ser. A*, *343*, 205–306, 1993.

Wilson, C. J. N., and W. Hildreth, The Bishop Tuff, new insights from eruptive stratigraphy, *J. Geol.*, *105*, 407–439, 1997.

Wilson, C. J. N., and G. P. L. Walker, The Taupo eruption, New Zealand, I, General aspects, *Philos. Trans. R. Soc. London Ser. A*, *314*, 199–228, 1985.

Wilson, L., Explosive volcanic eruptions, III, Plinian eruption columns, *Geophys. J. R. Astron. Soc.*, *45*, 543–556, 1976.

Wilson, L., R. S. J. Sparks, and G. P. L. Walker, Explosive volcanic eruptions, IV, The control of magma properties and conduit geometry on eruption column behavior, *Geophys. J. R. Astron. Soc.*, *63*, 117–148, 1980.

Woods, A. W., The fluid dynamics and thermodynamics of eruption columns, *Bull. Volcanol.*, *50*, 169–193, 1988.

Woods, A. W., The dynamics of explosive volcanic eruptions, *Rev. Geophys.*, *33*, 495–530, 1995.

Woods, A. W., and S. Bower, On the decompression of volcanic jets, *Earth Planet. Sci. Lett.*, *131*, 189–205, 1995.

Woods, A. W., and M. I. Bursik, Particle fallout, thermal disequilibrium and volcanic plumes, *Bull. Volcanol.*, *53*, 559–570, 1991.

Woods, A. W., and C. P. Caulfield, A laboratory study of explosive volcanic eruptions, *J. Geophys. Res.*, *97*, 6699–6712, 1992.

C. Jaupart and É. Kaminski, Laboratoire de Dynamique des Systèmes Géologiques, IPG Paris - Université Paris 7, 4 Place Jussieu, 75252 Paris cédex 05, France. (cj@ccr.jussieu.fr; kaminski@ipgp.jussieu.fr)

(Received August 1, 2000; revised December 14, 2000; accepted March 28, 2001.)